Experimental Observations of Mode Coupling from Injun 3 VLF Data*

by

Paul Rodriguez

A thesis submitted in partial fulfillment of the requirements for the degree of Master of Science in the Department of Physics and Astronomy in the Graduate College of The University of Iowa

June, 1969

Thesis Supervisor: Associate Professor Donald A. Gurnett

*Supported in part by the National Aeronautics and Space Administration under Contract No. NGR-16-001-043 and the Office of Naval Research under Contract No. Nonr 1509(06).

Graduate College
The University of Iowa
Iowa City, Iowa

CERTIFICATE OF APPROVAL

MASTER'S THESIS

This is to certify that the Master's Thesis of

Paul Rodriguez

with a major in Physics has been approved by the Examining Committee as satisfactory for the thesis requirement for the Master of Science degree at the convocation of June 6, 1969.

Thesis committee Donald O. Gunnett
Thesis supervisor

William N. Klink
Member

Fran W. Sh
Member

ACKNOWLEDGEMENTS

The author wishes to thank Dr. D. A. Gurnett for his encouraging and helpful advice during this study.

Thanks are also due to the other teachers, graduate students, and staff workers who helped with the necessary details.

7577-3

ABSTRACT

D. Jones has recently presented a theory of the effect of collisions on ion cyclotron whistlers. For propagation along the magnetic field, he derives criteria for mode coupling based on the wave normal angle of whistlers with respect to a critical coupling angle. He presents a theoretical distribution of mode coupling between electron and ion whistlers as a function of magnetic latitude, altitude, and temperature. In this paper, this distribution is confirmed on the basis of experimental data from satellite Injun 3. Some additional effects found in the real ionosphere are also noted: the auroral zone cutoff, possible turbulence effects in the summer-day ionosphere, and the general spread in coupling type occurrences so that distinct boundaries between the various coupling types do not exist.

Possible areas of related study are mentioned: ELF mode coupling and its relation to whistlers, the calculation of collision frequencies, and coupling effects for propagation perpendicular to the magnetic field.

TABLE OF CONTENTS

LIST OF FIGURES

LIST OF FIGURES (CONT.)

LIST OF FIGURES (CONT.)

I. INTRODUCTION

A. Statement of the Problem

In a cold multicomponent plasma with a magnetic field, two transverse modes of propagation are possible. In the direction of the magnetic field, these modes are right (R) and left-hand (L) circularly polarized. If the plasma parameters such as ion densities, plasma frequency and magnetic field are functions of position, then certain functions can be constructed in terms of these parameters which define surfaces in space. These surfaces indicate the places where the propagation characteristics change abruptly. At one of these parameter surfaces, identified by the equation $D = 0$, polarization reversal occurs for propagation in the direction of the magnetic field. Thus, a right-hand circularly polarized wave incident on one side of $D = 0$ becomes a left-hand circularly polarized wave on the other side. If the plasma parameters include collision frequencies, then mode coupling between the two modes is possible so that both modes propagate on the other side of $D = 0$.

This paper reports the results of an investigation of mode coupling by VLF ionospheric whistlers, as observed by Injun 3 satellite. The right (R) and left-hand (L) modes are identified as

electron and proton whistlers, following previous use [Storey, 1953; Smith et al., 1964; Gurnett et al., 1965].

B. Previous Work

Mode coupling by whistlers has been considered recently by Gurnett, Shawhan, Brice and Smith [1965] (hereafter referred to as GSBS) and by D. Jones [1968].

GSBS describe mode coupling in terms of a critical angle θ_c between the magnetic field and the direction of propagation. An upgoing electron whistler propagating near the cone of angles defined by θ_c becomes coupled to the ion whistler generated by crossing D = 0. For the model used by GSBS, θ_c is of the order of 10°.

Jones considers the model of GSBS with collision frequencies defined explicitly and derives criteria for critical coupling between the whistler modes.

II. THEORY OF MODE COUPLING

A. Inhomogeneous Anisotropic Medium

Forsterling's coupled equations for vertical incidence are the general expressions for the wave fields in an inhomogeneous, anisotropic medium [Budden, 1961]:

$$F_o'' + F_o(n_o^2 + \psi^2) = \psi' F_x + 2\psi F_x' \qquad (1)$$

$$F_x'' + F_x(n_x^2 + \psi^2) = \psi' F_o + 2\psi F_o'$$

F_o and F_x are proportional to the fields in the ordinary and extraordinary modes, respectively. The prime denotes $1/K\ \partial/\partial z$, where $K = n\omega/c$ is the wave number and Z is the vertical direction. n_o and n_x are the indices of refraction for the respective modes, and ψ is the "coupling parameter," so called because when $\psi = 0$ the equations are independent and the two modes propagate independently, while if $\psi \neq 0$ the equations are coupled and there is interaction between the modes. ψ has the form

$$\psi = \frac{\rho_o'}{(\rho_o^2 - 1)} = \frac{\rho_x'}{(\rho_x^2 - 1)} \qquad (2)$$

where ρ is the polarization, E_y/E_x, defined in terms of the components of the electric field which lie in the wavefront.

Forsterling's equations are of second order so four characteristic solutions are possible. Clemmow and Heading [1954] extend the general theory and use four independent variables for the four characteristic waves. The medium is considered to be horizontally stratified. These characteristic waves are the upgoing ordinary and extraordinary modes and the downgoing ordinary and extraordinary modes.

If the parameters of the medium are slowly varying, i.e., the medium is approximately homogeneous, the coupling terms are small and the WKB method can be used to obtain the four characteristic solutions. The criteria for determining "slowly varying" can be expressed in terms of the index of refraction,

$$\frac{1}{n^2} \frac{\partial n}{\partial z} \frac{\omega}{c} \ll 1.$$

That is, the relative change in the index of refraction over one wavelength should be small. This condition is violated if $n \to 0$ or $\partial n/\partial z$ is large.

At the VLF frequencies of interest (0-700 cps) the free space wavelength is of the order of 300 km, while in the ionosphere conditions often change over distances of less than one kilometer.

Clearly, the medium is not slowly varying and the WKB solutions do not apply. In Forsterling's equations, this is indicated by large values of the coupling parameter Φ.

A solution for vertical incidence then requires a "full wave" approach. For this purpose Clemmow and Heading's first order equations are more practical. These equations are solved in thin, successive layers of the ionosphere with the boundary conditions that the coupled wave fields in each layer must join smoothly to those of the next layer. This requires a numerical solution with a computer. Inoue and Horowitz [1966] have provided such a solution in the lower part of the ionosphere. They also give explicit and comprehensive forms for the coupling coefficients.

B. Mode Coupling at D = 0

A cold plasma is defined as having ions and electrons at zero temperature (zeroth order motion is zero), homogeneous in space and immersed in a uniform static magnetic field. None of these characteristics really apply to the ionosphere, but the results of the model provide wave modes which are observable in the ionosphere, namely the R and L modes.

The following quantities are defined for a cold plasma [Stix, 1962]:

$$R = 1 - \sum_k \frac{\Pi_k^2}{\omega(\omega + \epsilon_k \Omega_k)} \tag{3}$$

$$L = 1 - \sum_k \frac{\Pi_k^2}{\omega(\omega - \epsilon_k \Omega_k)} \tag{4}$$

$$P = 1 - \sum_k \frac{\Pi_k^2}{\omega^2} \tag{5}$$

$$S = \frac{1}{2}(R + L) \tag{6}$$

$$D = \frac{1}{2}(R - L) \tag{7}$$

$$\Pi_k^2 = \frac{4\pi n_k Z_k^2 e^2}{m_k} \tag{8}$$

$$\Omega_k = \frac{Z_k e B_o}{m_k c} \tag{9}$$

The subscript k refers to the kth species of charged particle.

The terms represent the following:

Π_k = plasma frequency (sec^{-1})

Ω_k = gyrofrequency (sec^{-1})

n_k = number density (cm^{-3})

ω = wave frequency (sec^{-1})

Z_k = charge number

e = electron charge (esu)

B_o = static magnetic field (gauss)

m_k = mass (gm)

c = vacuum speed of light ($cm\ sec^{-1}$)

Equations (3) - (7) are the parameter surfaces mentioned previously. They have the units of index of refraction squared (n^2). Equations (3) and (4) are shown by Stix to be the indices of refraction squared which correspond to the right and left-hand modes, hence the use of R and L.

From equation (7), the parameter surface D = 0 occurs when R = L. Stix and GSBS show that D = 0 has a solution only when the plasma has positive ions of different charge to mass ratios and for frequencies between the ion gyrofrequencies. For an ionosphere model which consists of electrons, and singly ionized hydrogen, helium, and oxygen, the frequency at which D = 0 between the H^+ and He^+ gyrofrequencies is called the cross-over frequency, ω_{12}. Between the He^+ and O^+ gyrofrequencies, the cross-over frequency is ω_{23}. These frequencies, along with the parameter surfaces of interest, are shown in Figure 1, which is reproduced from GSBS.

The polarization of the transverse modes in a cold plasma is given by GSBS as

$$\rho = \frac{iDn^2 \cos\theta}{Sn^2 - RL} \tag{10}$$

where θ is the angle between the wavefront normal and the static magnetic field. Along the magnetic field ($\theta = 0$) the polarization for $n^2 = R$ (electron whistler) is

$$\rho = +i$$

and for $n^2 = L$ (proton whistler) is

$$\rho = -i$$

which shows that the polarizations are right and left-hand circular.

As described by GSBS, the history of a whistler begins with a lightning flash below the ionosphere. All frequencies are generated in random polarizations, propagating outwards from the flash. Due to the large value of the index of refraction for the ionosphere, all waves penetrating into the ionosphere are refracted into nearly

vertical directions. At higher latitudes, the magnetic field in the ionosphere is also nearly vertical, so the conditions exist for the two transverse modes R and L. Random polarizations are thus decomposed into the R and L modes.

The plasma parameters in the lower ionosphere are such that in this region the L mode is evanescent and thus the upgoing L mode is immediately absorbed, leaving only the R mode. The regions of interest in the ionosphere with the bounding parameter surfaces are shown in Fig. 2. For a wave of frequency 400 cps, D = 0 occurs at an altitude of about 800 km. At this altitude, an electron whistler traveling along the magnetic field is changed into a proton whistler of the same frequency. At a higher altitude, the proton whistler is absorbed in resonance at L = ∞ where the proton gyrofrequency becomes equal to 400 cps.

Figure 1 shows that at D = 0 the gradient of the index of refraction changes abruptly from that of R to that of L. This leads to rapid changes of polarization with height and thereby to a large coupling parameter ψ. This indicates the possibility of mode coupling and reflections.

Physically, the coupling interaction takes place when the medium parameters are such that the phase velocities of the two modes become equal. This allows a division of the wave energy between the two available modes of propagation and we say that coupling has occurred. In the collisionless case the phase velocities of the R and L modes are

equal only along the $\theta = 0°$ direction, when D = 0 is crossed. This constitutes a singular point. When collisions are included, the angle at which the phase velocities are equal moves away from $\theta = 0°$ (to θ_c) and the coupling interaction broadens from a singular point to a finite range about θ_c. The indices of refraction are complex, but the real part remains the same as in Fig. 1 so that polarization reversal still occurs in a smooth manner. The relationship between coupling and polarization reversal can be confusing. They are related through the coupling parameter Ψ and coupling is possible any time the polarization changes rapidly, but the reversal is a property of the multicomponent plasma and is not due to coupling.

Budden (p. 334) shows that if the WKB approach is valid, then no reflections occur at a discontinuity in the gradient of the index of refraction; if the WKB approach is not valid, as in the case being considered, then it is not possible to define a purely upgoing wave near the discontinuity and the problem of reflections at the discontinuity has no meaning. Therefore, we consider that only coupling takes place at D = 0.

Collisions can be included in the plasma equations (3) - (9) by making the following changes in the formalism:

$$m_k \rightarrow m_k\left(1 + i\frac{\nu_k}{\omega}\right) \quad . \tag{11}$$

ν_k is the collision frequency of the kth particle.

With collisions included the polarization can be expressed by an equation due to Jones,

$$\rho^2 + \frac{2i}{G} \frac{\sin^2\theta}{\cos\theta} \rho + 1 = 0 \qquad (12)$$

where

$$G = \frac{P(L-R)}{RL-PS} \quad .$$

The roots of (12) are the polarization of the R and L modes,

$$\frac{\rho^{\pm}}{i} = \frac{-\sin^2\theta}{G\cos\theta} \pm \left[\left(\frac{\sin^2\theta}{G\cos\theta} \right)^2 + 1 \right]^{1/2} . \qquad (13)$$

The critical coupling angle θ_c can then be obtained from (13) when the roots are equal, or when

$$G = \pm i \frac{\sin^2\theta}{\cos\theta} \quad . \qquad (14)$$

This requires that the real part of G become equal to zero. The critical coupling condition can be displayed graphically by plotting equation (13) on the complex polarization plane. Figure 3 is taken from Jones and is for altitudes near the cross-over altitude, where D = 0 occurs for a given frequency. The model of GSBS has been used to evaluate G. The upper portion in the figure is for the L mode and the lower is for the R mode. (Jones used the definition $\rho = -i$ for right-hand polarization, $\rho = +i$ for left-hand) Thus, for an upward traveling wave in the R mode, with frequency 400 cps and wave normal angle 10°, the polarization changes over smoothly to the L mode at an

altitude of about 772 km. For $\theta = 8°$, the polarization changes with altitude but remains in the R mode. In both cases, no mode coupling occurs since the coupling parameter ψ remains small and may be neglected. Therefore, only one mode exists on either side of D = 0.

For $\theta = \theta_c = 8.9°$ the R mode crosses the axis at $\rho = 1$ where the roots are equal, $\psi \to \infty$, and critical coupling occurs. The upward traveling R mode, on one side of D = 0, is split into R and L modes on the other side of D = 0. The amplitudes of the R and L modes relative to the original R mode are given by the coupling coefficients. As stated previously, a full wave solution is necessary to obtain these coefficients. At higher altitudes both modes exist until the L mode is absorbed at $L = \infty$. In Fig. 2, the cross-hatched region between D = 0 and $L = \infty$ is where both modes are possible.

For polarization curves that pass close to the critical coupling point (within the dotted circle in Fig. 3) the polarization approaches the value 1 and is changing rapidly. Both these effects make ψ large, so that weak coupling can occur with the generation of a small amount of the coupled mode.

We can now state the criteria for coupling in terms of the wave normal angle and the critical angle:

(a) $\theta > \theta_c$. No coupling. An upward traveling R mode changes smoothly into the L mode. If $|\theta - \theta_c|$ is small, weak coupling may generate a small amount of the R mode.

(b) $\theta = \theta_c$. Critical coupling. An upward traveling R mode is split into R and L modes. The relative amplitudes are given by coupling coefficients.

(c) $\theta < \theta_c$. No coupling. An upward traveling R mode remains in the R mode. If $|\theta - \theta_c|$ is small, weak coupling may generate a small amount of the L mode.

The coupling criteria also apply for waves traveling downward. The presence of the parameter surface L = 0 below D = 0 includes a new effect, however. Stix shows that, generally, reflections occur where parameter surfaces have the value zero (index of refraction = 0) and absorption where the surfaces have infinite value (index of refraction $\rightarrow \infty$). Therefore, an R mode with $\theta > \theta_c$ incident on D = 0 from above changes over to the L mode, proceeds a little farther and is reflected off L = 0. An L mode with $\theta > \theta_c$ incident on D = 0 from above changes into the R mode and is transmitted past L = 0 into the lower ionosphere. For

$\theta = \theta_c$, either R or L modes incident on D = 0 from above allows both modes to exist in the region between L = 0 and D = 0.

For a given altitude in the ionosphere, Fig. 2 gives the range of frequencies in which the proton whistler will be observed, between the cross-over frequency ω_{12} and the proton gyrofrequency Ω_1. This will be true if polarization reversal has occurred. On either side of this range, $\omega_{12} - \Omega_1$, only the electron whistler should be observed. If mode coupling has occurred, then both modes should be present in the range $\omega_{12} - \Omega_1$. In an actual recording of these signals they can be identified by their difference in phase velocities. The L mode travels slower than the R mode so an antenna would detect the L mode after the R mode in the given range of frequencies. As the L mode approaches the altitude where resonance occurs, the phase velocity approaches zero and is detected a longer and longer time after the R mode. Figure 4 shows the type of trace expected on frequency-time axes.

Figure 3 is computed for one wave frequency, 400 cps. For the range 0-700 cps, the critical angle θ_c changes along the surface D = 0. Using the model of GSBS, Jones obtains a minimum angle of $\theta_c = 5°24'$ at about 1600 km. Therefore, if we assume that in the range of frequencies of a dispersed electron whistler the wave normal angle is constant, at a given altitude the critical angle

may be less than, or greater than, or equal to the wave normal angle. This will cause portions of the electron whistler between ω_{12} and Ω_1 to remain in the R mode while other portions in the same range are changed to the L mode. The result is that the proton whistler appears to be partially formed. Figure 5 shows a plot of critical angles as calculated by Jones versus the frequencies of interest. Thus, for a wave normal angle $\theta_1 = 10°$, the frequency range beyond about 410 cps remains in the R mode. For $\theta_2 = 7°$, only the central portion of the frequency range has polarization reversal.

At high latitudes, the earth's magnetic field in the ionosphere becomes more nearly vertical, so for upward traveling electron whistlers, the wave normal angles are small and may lie inside the critical coupling cone. This leads to the expectation that proton whistlers should progress from fully formed at low latitudes, to partially formed at higher latitudes, to an eventual cutoff at high latitudes. There are thus two effects leading to partially formed proton whistlers, one frequency dependent, the other latitude dependent. Experimentally, it is difficult to separate the two and was not attempted in this study.

III. OBSERVATIONS OF MODE COUPLING

A. Data Sample

Injun 3 satellite was launched into orbit on December 13, 1962. The orbit had an apogee of 2785 km, perigee of 236 km and period of 116 minutes. The orbital plane was inclined at 70.4° to the equatorial plane. Information transmission lasted until the end of October, 1963. The lifetime of the satellite was characterized by low magnetic activity.

The experimental data consisted of spectrograms similar to Fig. 4. A total of 277 spectrograms were used, 158 for winter-night and 119 for summer-day. (See Fig. 8a for the definitions of winter-night and summer-day.) Part of this sample was used previously for a study of the fractional concentration of hydrogen ions [Shawhan and Gurnett, 1966]. In that study, measurements of the ratio ω_{12}/Ω_1 were sought so it was necessary that the proton whistler be visible. Therefore, samples in which only the electron whistler was visible, i.e., coupling type C_5, were not included. It was thus necessary to adjust the sample for this coupling type.

The original sample was obtained by analyzing all the satellite passes for the 11th and 26th of the month during winter-night and summer-day. (A pass is the part of a satellite revolution during

which data have been recorded on magnetic tape by a particular station.) For a satellite lifetime of 10 months, this gave about 20 days of data over a reasonably uniform range of altitude, local time, and latitude. The data tapes were played back through an audio amplifier and recorder (Sonograph, Kay Electric) from which the spectrograms were made. Proton whistlers were then picked at random. In this case, "at random" implies that the proton whistler had to be strong enough to be heard, so that very weak proton whistlers were not considered.

The resulting sample constituted about 10% of all the proton whistlers that were recorded on the given passes. This number was determined by reviewing the passes used by Shawhan and Gurnett. Spectrogram films of the data were available to allow a considerable saving of time. Whistler bursts were not included in the count because it is not possible to determine accurately whether any proton whistlers are occurring when electron whistlers are spaced very closely together.

Over the same passes, then, about 10% of the electron whistler occurrences, coupling type C_5, where picked at random. Some further adjustment was later necessary since orbital data was not always available for a pass or for part of one.

It was also decided to obtain samples at higher latitudes in both hemispheres. The procedure was to analyze data for passes during winter-night and summer-day for two high latitude stations, College, Alaska and Woomera, Australia. For these stations, passes on the 11th and 26th of the month (or as close to those days as possible) were taken. Spectrograms were then made of approximately 10% of the whistler occurrences, picked at random. It is felt that this gives a reasonably complete coupling type distribution in the sample.

B. Classification of Coupling

For the purpose of this study, coupling is classified according to the scheme given in Fig. 6. C_1 represents the case of a smooth transition from the R mode to the L mode, with none of the R mode present between frequencies ω_{12} and Ω_1. This means that $\theta > \theta_c$ and corresponds to a path like $E \rightarrow E'$ in Fig. 3. C_2 is the weak coupling case, $|\theta - \theta_c|$ is small, and a small amount of the R mode is generated between ω_{12} and Ω_1. C_3 is the critical coupling case, $\theta = \theta_c$. Both modes are present between ω_{12} and Ω_1. C_4 represents weak coupling with a small amount of the L mode between ω_{12} and Ω_1 and C_5 is the no coupling case, similar to C_1.

In Fig. 7, actual spectrograms of these coupling classifications are given. These samples are all winter-night occurrences covering a broad latitude range.

The coupling type classification is based, of course, on the appearance of the spectrograms. The coupling type assigned to a particular event was based on the relative intensity of the electron and proton whistler traces between frequencies ω_{12} and Ω_1. This assumes that the relative intensity as shown on the spectrograms are proportional to the relative intensities as they occurred in the ionosphere. Physically, the satellite detected a whistler through a loop antenna sensitive to the magnetic component of the electromagnetic wave [Gurnett and O'Brien, 1964]. The loop antenna and preamplifier then presented a signal to the wideband (0.5 - 7.0 kcps) VLF system from which high resolution frequency-time spectrums were telemetered to the ground. The frequency response of the wideband VLF system to the voltage signals in the frequency range of interest changed by no more than 10 db. Since the coupling type is based on signal intensities in the same frequency range, ω_{12}-Ω_1, both modes are affected equally by the wide-band VLF system and should retain their relative intensities unchanged.

Coupling type C_5 does not show any proton whistler (L mode). It is assumed that this is due to either one or both of two things:

the wave normal angle is less than the critical angle, or the D = 0 surface has not been crossed. On the basis of the model of Fig. 2, we expect that for the range of altitudes covered, the lowest frequency waves cross D = 0 at the highest altitudes. Therefore, for medium satellite altitudes, the whistler mode in the lowest frequencies should be R (right-hand). The lowest cross-over frequency both in the model and in the sample is of the order of 200 cps. Thus, if only the electron whistler is observed (R mode) down to the lowest frequencies, we can be fairly certain that D = 0 has been crossed and that the L mode is missing because the wave normal angle was less than critical. If the electron whistler does not reach the lowest frequencies, we cannot tell if D = 0 is crossed. Cases like this were excluded from the sample. There are examples, however, of the situation where the electron whistler is cutoff at frequencies of the order of 500-600 cps, with the proton whistler appearing between ω_{12} and Ω_1. In terms of their model, GSBS have attributed this cutoff of the electron whistler to the merging of the D = 0 and L = ∞ surfaces at about 700 cps. If we consider an upward traveling electron whistler to be changed entirely into a proton whistler at D = 0, then frequencies in the L mode between the electron whistler cutoff frequency, Ω_c, and the proton gyrofrequency at the altitude of the satellite are absorbed at L = ∞ and never

reach the satellite. Frequencies below the proton gyrofrequency would be detected in the L mode and this corresponds to coupling type C_1.

The spectrogram sample was divided into two categories according to the time of occurrence, during winter-night (WN) or summer-day (SD). This represents the extremes in ionospheric temperatures and gives a measure of the temperature dependence of mode coupling. Particle temperature affects coupling through the change in the collision frequencies involved. The change in the cold plasma formalism made in equation (11) assumes that collisions introduce a velocity dependent drag force in the particle dynamical equations [Stix, 1962]. The functional forms of ν_k that have been used by various authors are generally complicated and different for different species. Jones [1968] gives a summary of these functionals. Except for collisions between neutrals and ions, the collision functions are all temperature and density dependent. Generally, the collision frequencies increase with increasing ion density and decreasing temperature, and vice versa. Therefore, winter-night corresponds to large collision frequencies (moderate ion density, low temperature) and summer-day corresponds to small collision frequencies (low densities, high temperatures). The dates and times for winter, summer-day and night are given in Fig. 8a. This figure also shows the sample

distribution in terms of magnetic latitude and local time. The sample was picked to correspond to the more stable conditions of winter-night and summer-day. This occurs near dawn and dusk when the ionospheric has cooled or heated between 6 and 12 hours.

To obtain the coupling dependence on altitude and magnetic latitude, the meridional plane was divided into data boxes of 400 km altitude intervals and 10° magnetic latitude intervals. This includes the lower altitude and latitude limits for proton whistler occurrence (440 km, 0° - 10°) as reported by Shawhan [1966]. In each of these data boxes, the frequencies of occurrence of each coupling type was calculated, for winter-night and summer-day. Ideally, this determines the functional dependence of mode coupling on temperature, altitude, and magnetic latitude. The number and distribution of coupling types in these data boxes is shown in Fig. 8b.

C. Discussion of Results

The frequency of occurrence for the ith coupling type was calculated using the equation

$$f(C_i) = \frac{n(C_i)}{\sum_{i=1}^{5} n(C_i)} \qquad (15)$$

where $n(C_i)$ is the number of samples of coupling type C_i occurring within a given data box. This number ranged from 28 down to zero. This presented the problem of the relative importance that should be given to the frequency of occurrence calculated for a data box with a small number of samples. Numerous data boxes occurred that had only one, two, or three samples in them. Sometimes these were all of the same coupling type so that for these, $f(C_i) = 1.00$, yet the small number of samples did not inspire confidence in this value of $f(C_i)$. On the other hand, the small sample number indicates that on the particular satellite pass (or passes) in which the sample occurred, there was a low level of whistler activity and therefore a larger sample number was not possible. With this point of view, even the data boxes without samples are significant for they show that whistler activity in these regions was low during the particular pass.

With the preceding argument as a guide then, it was decided that while major consideration would be given to data boxes with the larger number of samples, those with small sample number would not be ignored completely, but would be used as a weighting factor whenever a decision had to be made about which way the curves for frequency of occurrence should turn, in the absence of better information. This requires a certain amount of interpretation that would not be necessary with a larger sample size.

Smooth curves were drawn through the maximum frequencies of occurence for each coupling type to give the curves of Figs. 9 and 10. These contours should be compared with Jones' Figs. 7 and 11, calculated on the basis of the model of GSBS. It is seen that the general nature of the curves are similar, with the winter-night curves reaching lower in altitude and turning upwards sooner with increasing latitude than do the summer-day curves. There is a general progression of coupling type with latitude, C_1 occurring at lower latitudes, C_5 at higher latitudes. The winter-night contours show this more clearly than do the summer-day contours with the maximums in the various coupling types being well separated from each other. For the summer-day contours the maximums are closer together and possibly reflect more turbulent conditions associated with higher ionospheric temperatures. Thus, over many satellite passes, the positions of the summer-day contours may change so often that the average position of each curve turns out to be approximately the same.

There are some important differences between Figs. 9 and 10 and the curves of Jones that should be noted. First, we see that neither the winter-night nor summer-day curves extend to as high a latitude as do the curves of Jones. Samples were taken from the higher latitude stations especially to look for this extension.

In all cases, the whistler activity much above 60° magnetic latitude was very low or non-existent. The cutoff in whistler activity thus seems to be definitely around 60° magnetic latitude, and is associated with the beginning of the auroral zone [Shawhan, 1966]. That Jones' curves do not show this cutoff is due to his use of the ionosphere model of GSBS, which does not include any effect due to the auroral zone.

Also, the small latitude range between fully formed proton whistlers and no proton whistlers which Jones' curves show is not present in the winter-night curves obtained in this study, Fig. 9. Figure 10 does show such an apparent small latitude range, but this may be due to the other effects previously mentioned. In any case, Fig. 9 indicates that instead of "sharp" transitions in coupling types, we have gradual transitions from one type to another over a broad range of latitudes. Further, since the curves represent statistical averages, the contours in both Figs. 9 and 10 do not represent boundaries between coupling types as Jones' curves do. Figures 9 and 10 also indicate the observed result that at any given point, all five coupling types can occur. Numerous spectrograms were taken that showed different coupling types occurring within a few seconds of each other on the same satellite pass. Figure 9 shows one pass of the recently launched satellite Injun 5 (line AA')

with the coupling type subscript placed at the position of occurrence of a whistler. This pass is a typical example of what the expected coupling type distribution should be: more cases of C_5 occurring at high latitudes than any other, and more cases of C_1 occurring at low latitudes than any other, but all cases being possible at any given latitude.

Another distinction between Figs. 9 and 10 and Jones' curves is to be noted. The variation with latitude of the coupling type is to be expected, as Jones points out, on the basis of the change in direction of the magnetic field with increasing latitude, and the consequent change in the wave normal angle of a vertically propagating wave. Since most critical coupling angles are in the range 5° - 10°, at low latitudes the condition $\theta > \theta_c$ is more likely to occur while at high latitudes the condition $\theta < \theta_c$ is more probable. This leads to an expected coupling type distribution like Fig. 9. The change in wave normal angle can also lead to partially formed proton whistlers, and it is on this basis that Jones' curves are drawn. For a given proton whistler, partial formation indicates a change in coupling type along the range of frequencies between ω_{12} and Ω_1. On spectrograms, this would show up as a variation of intensity of the proton whistler compared with the electron whistler trace. Jones' curves, therefore, include a measure of the rate of

of change of the critical coupling angle between ω_{12} and Ω_1. Such a fine distinction of mode coupling was not easily observed in this study and was not attempted; therefore, Figs. 9 and 10 are a measure of the change in mode coupling only, and not of the rate of change in mode coupling, between ω_{12} and Ω_1. There were, however, some cases in which partial formation of the proton whistler was clearly evident. Figure 15 shows one example. However, for the most part, proton whistler traces did not exhibit marked variations of intensity along the trace, indicating that the critical coupling angle did not change very much between ω_{12} and Ω_1.

Finally, we mention that Jones' curves were calculated using the model of GSBS for ion and electron density distributions. This results in the D = 0 and L = ∞ parameter surfaces of Fig. 2. Figures 11 and 12 are plots of the experimentally measured values of ω_{12} and Ω_1 for winter-night and summer-day. The curves reproduce the D = 0 and L = ∞ surfaces as they exist in the ionosphere. It is evident that there is a latitude dependency in these curves which is not included in the model of GSBS and would effect the calculations of Jones' curves.

Figure 13 is of ω_{12} and Ω_1 for the latitude range 30° - 40°, winter-night. It shows the typical scatter of points in the

plots of Figs. 11 and 12. Figure 13 also shows the cutoff frequencies measured for electron whistlers. On the basis of the model of GSBS we would expect that the cutoff Ω_c should occur within a small range of frequencies around 700 cps for all altitudes. The experimental points indicate that cutoffs of the electron whistler do not occur regularly and that when they do, it is for a wide range of frequencies, sometimes even below Ω_1. The curves of Fig. 13 are very similar to those of the model used by GSBS, so we cannot attribute the irregular behavior of the cutoff frequencies to a serious error in the model. It is possible that the rapidly changing conditions near the lower boundary of the ionosphere has significant effects on the electron whistler cutoff which have not been considered.

It was previously mentioned that collision frequencies increased with the particle densities. Measurements of ion densities have been made which show that rapid changes can take place over periods of a day, so that it is possible to take this effect into account only in an average way. The winter-night, summer-day division of data was the most readily available way of considering ion densities.

Taylor et al., [1968] has made measurements of the light ion densities (H^+, He^+, O^+, N^+) using OGO-2 satellite. This satellite covered the altitude range 415-1523 km and during the

period October 14-24, 1965, the orbit was nearly along the dawn-dusk plane of the earth. Taylor et al., give measurements of the absolute ion densities [Fig. 2 of Taylor et al.] which thus exhibit the winter-night, summer-day dependency of interest here. Of particular interest is the observed high latitude trough in the light ion concentrations at around 60° magnetic latitude, corresponding with the observed whistler cutoff. The H^+ concentration measurements near 60° magnetic latitude on October 15, 1968 show a change from 10^4 ions/cm^3 to 10^2 ions/cm^3. Over a ten-day period this high latitude trough was a persistant feature of the composition. Figure 8a shows (cross-hatched region) the local time region covered by OGO-2 during the ten-day period. Since H^+ must be present for proton whistlers to occur, we see that the cutoff at high latitudes is a direct result of the effect the decreasing ion density has on the evaluation of the critical coupling angle.

IV. RELATED TOPICS

A. ELF Mode Coupling

In order to consider mode coupling in a more complete fashion, downward propagating waves should be included. A downward propagating R mode with $\theta > \theta_c$ is changed to the L mode on crossing the D = 0 surface. However, as shown in Fig. 2, the L = 0 parameter surface is encountered next. This means that the index of refraction for the L mode approaches zero rapidly and reflection of the L mode occurs. Gurnett and Burns [1968] use this mechanism to explain the low frequency cutoff of ELF emissions observed by Injun 3. At lower latitudes, the cutoff frequency is found to occur in almost all cases within the range $0.8\Omega_1 - \Omega_1$, decreasing steadily for increasing altitude. At higher latitudes the cutoff frequency dependence on altitude is less well defined. This is explained in terms of the wave normal angle θ. For values of $\theta > \theta_c$ reflection of the L mode occurs when the horizontal component of the refractive index vector n $\sin\theta$ becomes equal to the horizontal refractive index n_x of the ionosphere. Generally, this actually occurs above the L = 0 frequency but below the proton gyrofrequency. At higher latitudes, the condition $\theta > \theta_c$ is less likely to occur, the cutoff frequency is less well defined, and the R mode exists below L = 0.

This explanation for the cutoff of ELF emissions also implies that the emission source is above the maximum cutoff altitude. Gurnett and Burns locate a possible source near the equatorial plane at L values (McIlwain's geomagnetic shell parameter [1961]) of 4 to 8.

Usually, it is assumed that all whistlers are upgoing, since their spectrogram traces can be easily explained through the use of Fig. 2 for upward propagation. A different trace would be expected for downgoing whistlers. (Multiple hop whistlers are not included in this consideration; they can be identified by their greater dispersion.) Also, a pulse source is needed (lightning flash) and such a source at high altitudes seems unlikely. However, we can construct the sort of transitions that could be expected if a downgoing whistler should exist. By way of summary, Fig. 14 is a schematic diagram of the transitions that we have been considering for upgoing and downgoing whistlers. For the cases where reflections occur, Snell's law holds and therefore, the wave normal angle is the same for both incident and reflected waves. This preserves the coupling type through the reflection.

B. Collision Frequencies

In equation (11), it was assumed that the effect of collisions on the equations for a cold plasma was to introduce a velocity

dependent drag force into the dynamical equations. Therefore, for a multicomponent plasma, the drag on the jth particle due to the kth particle should be equal to the drag on the kth particle due to the jth particle. This is expressed by

$$n_j m_j \nu_{jk} = n_k m_k \nu_{kj} \tag{16}$$

[Stix, 1962], where ν_{kj} is the collision frequency between the kth and jth particles. For the kth species, the total collision frequency is then

$$\nu_k = \sum_j \nu_{kj} \tag{17}$$

and this is the value of ν_k that is required in equation (11). Using equation (16) it is possible to derive the following relation that could be of help in attempting an evaluation of (17):

$$\frac{\nu_{jk}\nu_{kl}}{\nu_{lk}\nu_{kj}} = \frac{\nu_{jl}}{\nu_{lj}} \tag{18}$$

We can also rewrite (16) (for j = e, electrons) in the form

$$\nu_{ek} = \left(\frac{n_k}{n_e} \right) \left(\frac{m_k}{m_e} \right) \nu_{ke}$$

$$= \alpha_k \mu_k \nu_{ke} \qquad (19)$$

where α_k is the fractional concentration of the kth ion and μ_k is the mass ratio. The quantity α_k has been calculated by Shawhan and Gurnett [1966] for H^+ in a collisionless plasma. They derive the equation

$$\alpha_1 = \frac{264}{255} \left[1 - \left(\frac{\omega_{12}}{\Omega_1} \right)^2 \right] \qquad (20)$$

where ω_{12} and Ω_1 may be measured from whistler spectrograms. The modification of (20) when collisions are included has not been derived and serves as a possible future study. A systematic approach requires that we start with the cold plasma equations (3) - (9).

C. Propagation Perpendicular to B

The R and L modes which have been studied in the preceding sections are identified for a wave normal angle of zero. For propagation perpendicular to the magnetic field ($\theta = \Pi/2$) the

two modes that can exist in a cold plasma are identified by the letters O and X (for ordinary and extraordinary). The dispersion equations for these modes are [Stix, 1962]

$$n_o^2 = P$$

$$n_x^2 = \frac{RL}{S} \tag{21}$$

where P, R, L, S have been defined already. These modes are linearly polarized. Similar to the R and L modes at D = 0, the phase velocities of the O and X modes become equal at a parameter surface identified by the equation RL = PS. On crossing this surface the modes exchange polarizations. There is thus the possibility of mode coupling. This problem has not been studied and serves as an area of future consideration.

V. CONCLUSIONS

The results of this study show that the coupling criteria and distribution for ion cyclotron whistlers as presented by Jones is confirmed experimentally.

It is expected that a similar study of helium whistlers will produce qualitatively the same results. (Figure 15 gives some samples of helium whistlers observed with Injun 3.) In this connection, it is recommended that the approach of such a study take the route of careful selection of individual satellite passes in which every event is analyzed rather than the random selection of individual whistlers. Such an approach serves to preserve the transitions in coupling type that may be lost when only individual whistlers are examined.

The existence of ELF mode coupling serves to demonstrate the general nature of the coupling phenomena in the frequencies below the electron gyrofrequency.

LIST OF REFERENCES

Budden, K. G., Radio Waves in the Ionosphere, Cambridge University Press, Cambridge, England, 1961.

Clemmow, P. C., and J. Heading, Coupled forms of the differential equations governing radio propagation in the ionosphere, Proc. Cambridge Phil. Soc., 50, 319, 1954.

Gurnett, D. A., and B. J. O'Brien, High-latitude geophysical studies with satellite Injun 3, 5. Very-low-frequency electromagnetic radiation, J. Geophys. Res., 69, 65-89, 1964.

Gurnett, D. A., S. D. Shawhan, N. M. Brice, and R. L. Smith, Ion cyclotron whistlers, J. Geophys. Res., 70, 1665, 1965.

Gurnett, D. A., and T. B. Burns, The low-frequency cutoff of ELF emissions, J. Geophys. Res., 73, 7437, 1968.

Inoue, Y., and S. Horowitz, Magneto-ionic coupling in an inhomogeneous anisotropic medium, Radio Sci., 1, (New Series), 427, 1966.

Jones, D., The theory of the effect of collisions on ion cyclotron whistlers, paper presented at the NATO Advanced Study Institute on Plasma Waves in Space and in the Laboratory, Røros, Norway, April 17-26, 1968.

LIST OF REFERENCES (CONT.)

McIlwain, C. E., Coordinates for mapping the distribution of magnetically trapped particles, J. Geophys Res., 66, 3681, 1961.

Shawhan, S. D., Experimental observations of proton whistlers from Injun 3 VLF data, J. Geophys. Res., 71, 29, 1966.

Shawhan, S. D., and D. A. Gurnett, Fractional concentration of hydrogen ions in the ionosphere from VLF proton whistler measurement, J. Geophys. Res., 71, 47, 1966.

Smith, R. L., and Neil Brice, Propagation in multicomponent plasmas, J. Geophys. Res., 69, 5029-5040, 1964.

Stix, T. H., The Theory of Plasma Waves, McGraw-Hill Book Company, New York, 1962.

Storey, L. R. O., An investigation of whistling atmospherics, Phil. Trans. Roy. Soc. London, A246, 113-141, July 9, 1953.

Taylor, Jr. H. A., H. C. Brinton, M. W. Pharo, III, and N. K. Rahman, Thermal ions in the exosphere; evidence of solar and geomagnetic control, J. Geophys. Res., 73, 5521, 1968.

FIGURES

Figure 1 Refractive index squared, parameter surfaces, and phase velocity surfaces for propagation in multi-component plasma. (GSBS model)

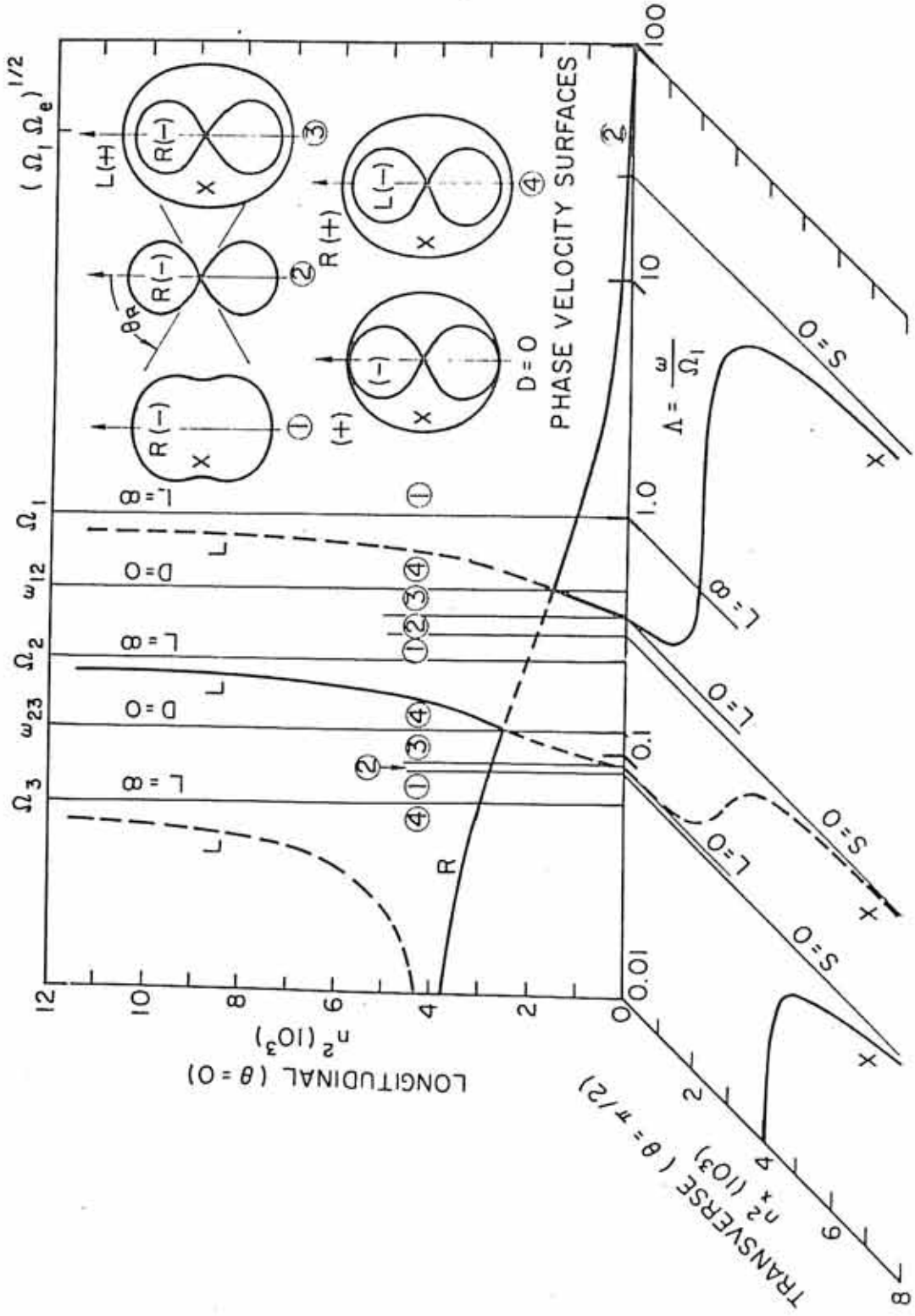
PHASE VELOCITY SURFACES
LONGITUDINAL (θ = 0)
TRANSVERSE (θ = π/2)
n² (10³)
n_x² (10³)
Λ = ω/Ω₁
L = 0
S = 0
L = ∞
S = ∞
D = 0
R(−)
L(+)
R(+)
L(−)
(+)
(−)
Ω₁
ω₁₂
Ω₂
ω₂₃
Ω₃
(Ω₁ Ω_e)^1/2

FIGURE 1

Figure 2 GSBS model ionosphere, parameter surfaces, and phase velocities at 400 cps.

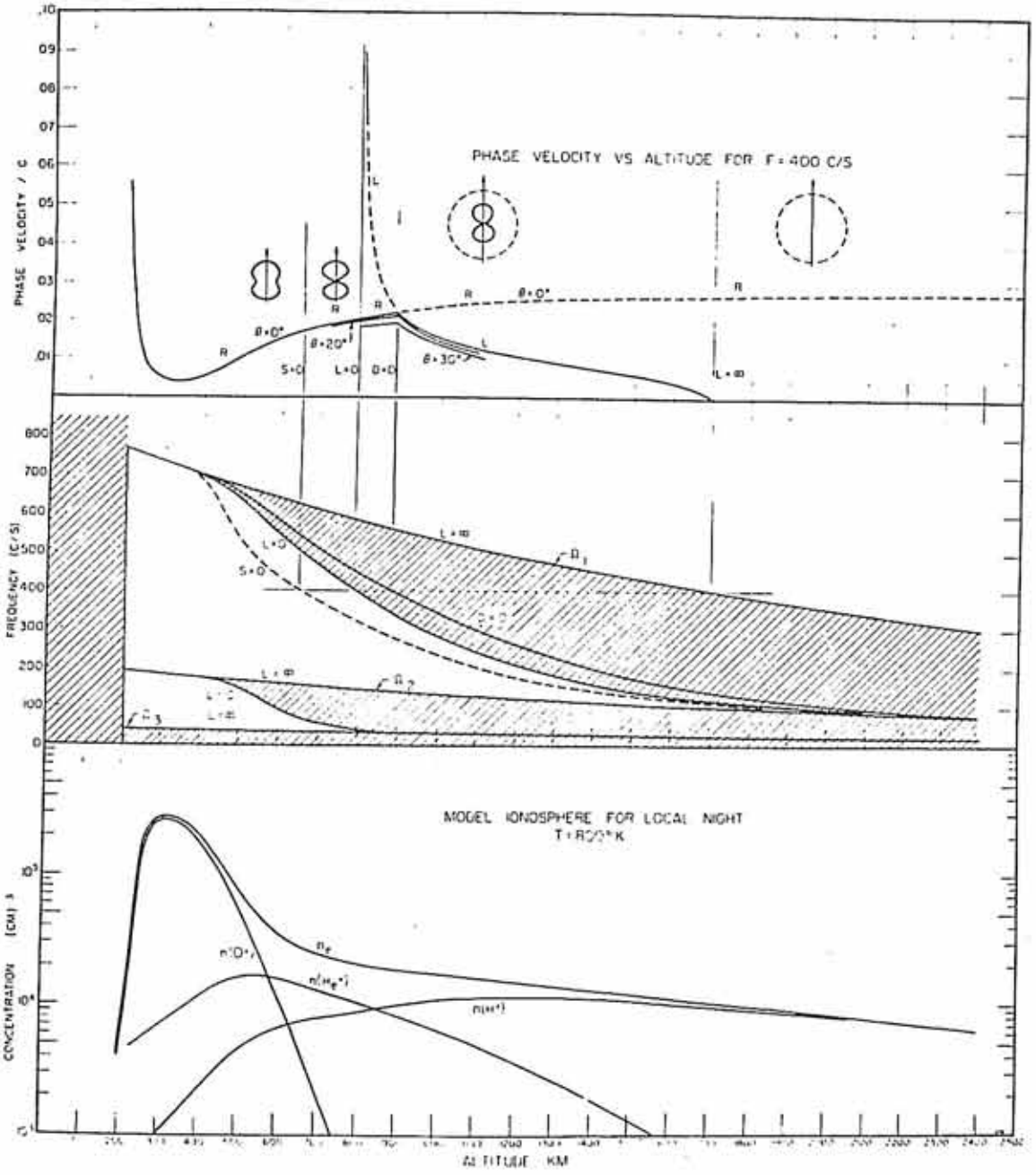
PHASE VELOCITY VS ALTITUDE FOR F = 400 C/S
PHASE VELOCITY / C
FREQUENCY (C/S)
MODEL IONOSPHERE FOR LOCAL NIGHT
CONCENTRATION (CM)
ALTITUDE KM

FIGURE 2

Figure 3 Variation of polarization [equation (13)] with wave normal angle θ and altitude, at 400 cps (Jones).

A-G69-177

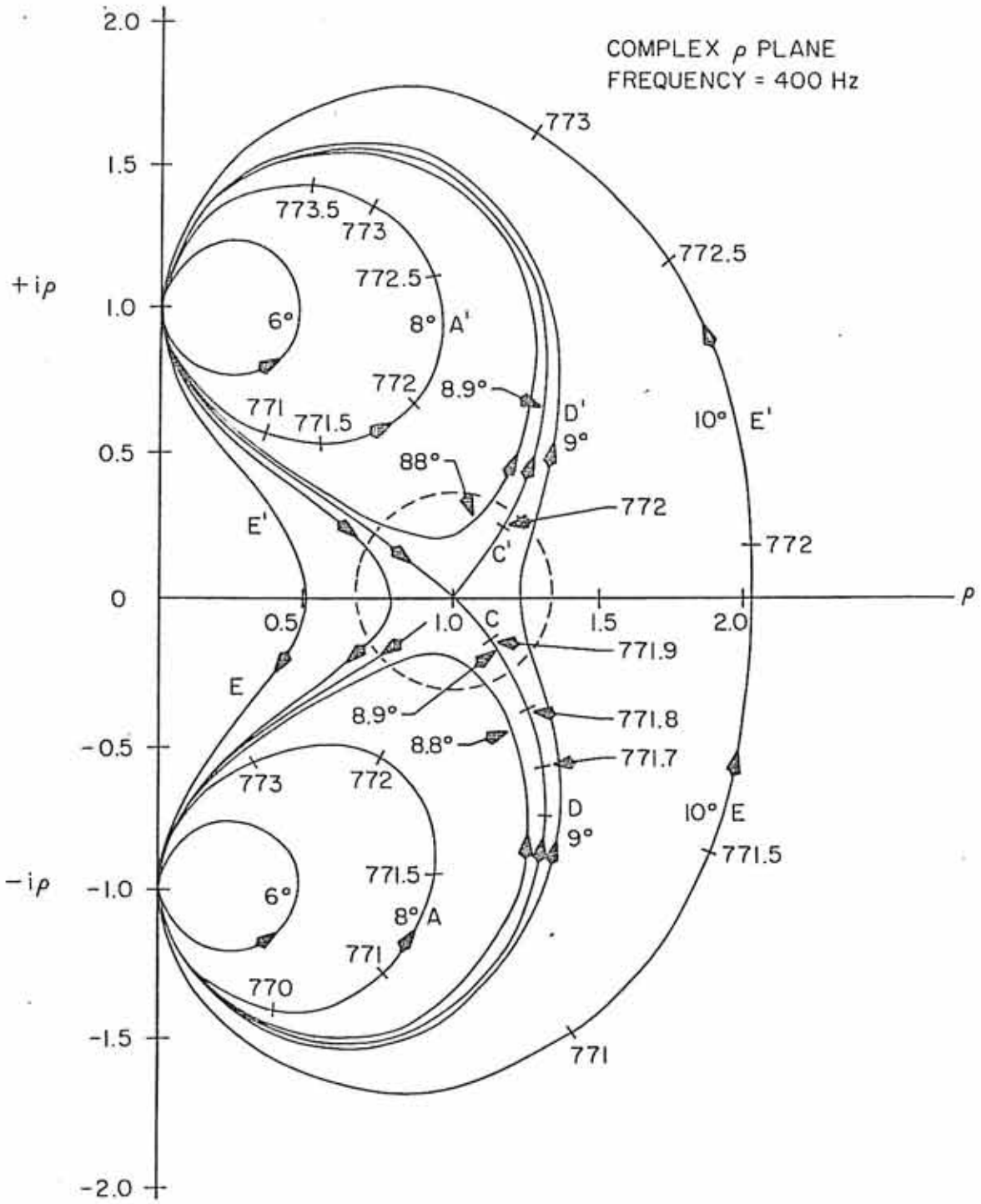

FIGURE 3

Figure 4 Proton whistler spectrogram. Ω_1 is the proton gyrofrequency, ω_{12} is the cross-over frequency, and Ω_c is the whistler cutoff frequency.

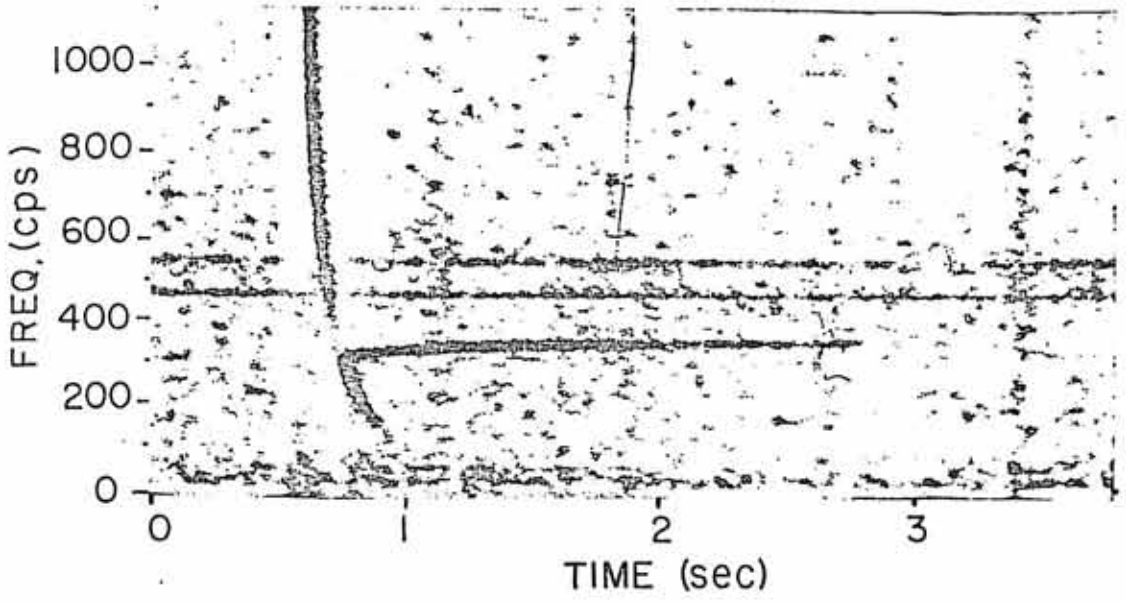
1000
800
600
400
200
0
FREQ. (cps)
0
1
2
3
TIME (sec)

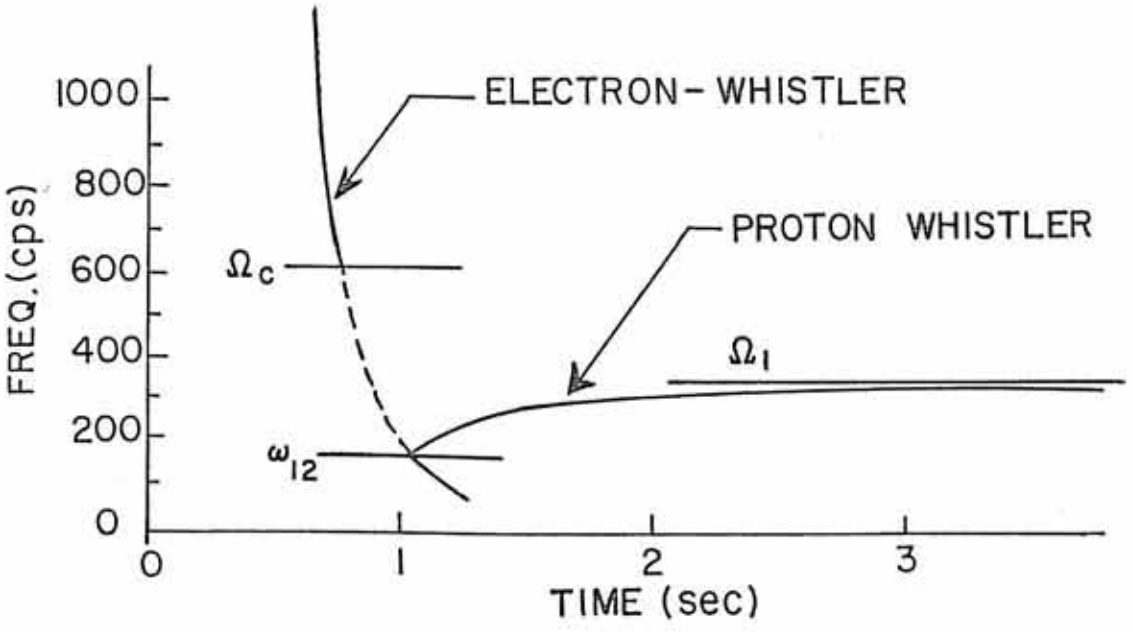
ELECTRON - WHISTLER
PROTON WHISTLER
Ω_c
Ω_1
ω_{12}
1000
800
600
400
200
0
FREQ. (cps)
0
1
2
3
TIME (sec)

FIGURE 4

Figure 5 Critical coupling angle as calculated by Jones versus the frequency range of interest.

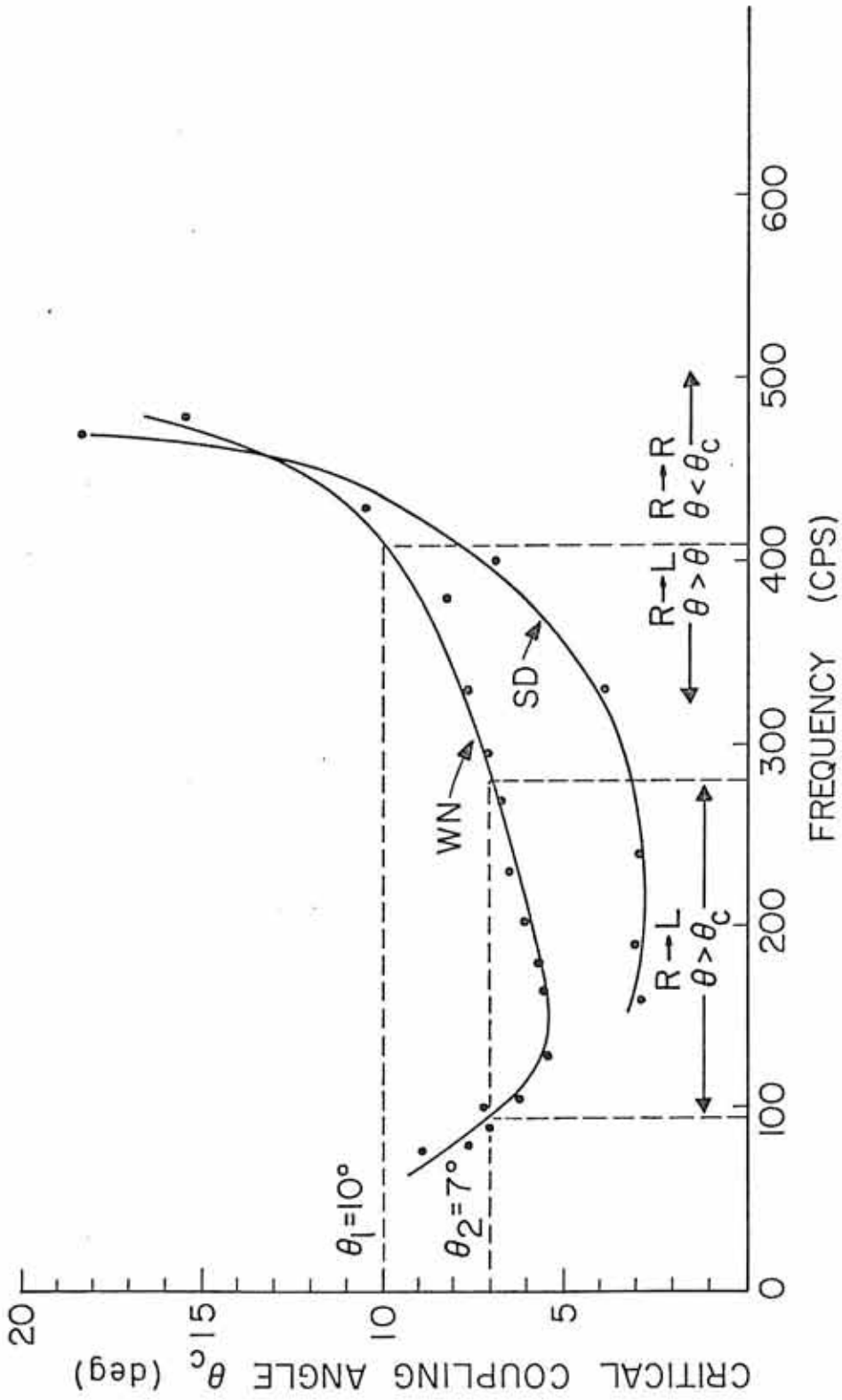
A-G69-187
CRITICAL COUPLING ANGLE θ_c (deg)
20
15
10
5
0
100
200
300
400
500
600
FREQUENCY (CPS)
θ_1=10°
θ_2=7°
WN
SD
R→L
$\theta > \theta_c$
R→L
$\theta > \theta$
R→R
$\theta < \theta_c$

FIGURE 5

Figure 6 Classification of coupling type based on the appearance of whistler spectrograms.

A-G69-173

CLASSIFICATION OF COUPLING TYPE, C_n

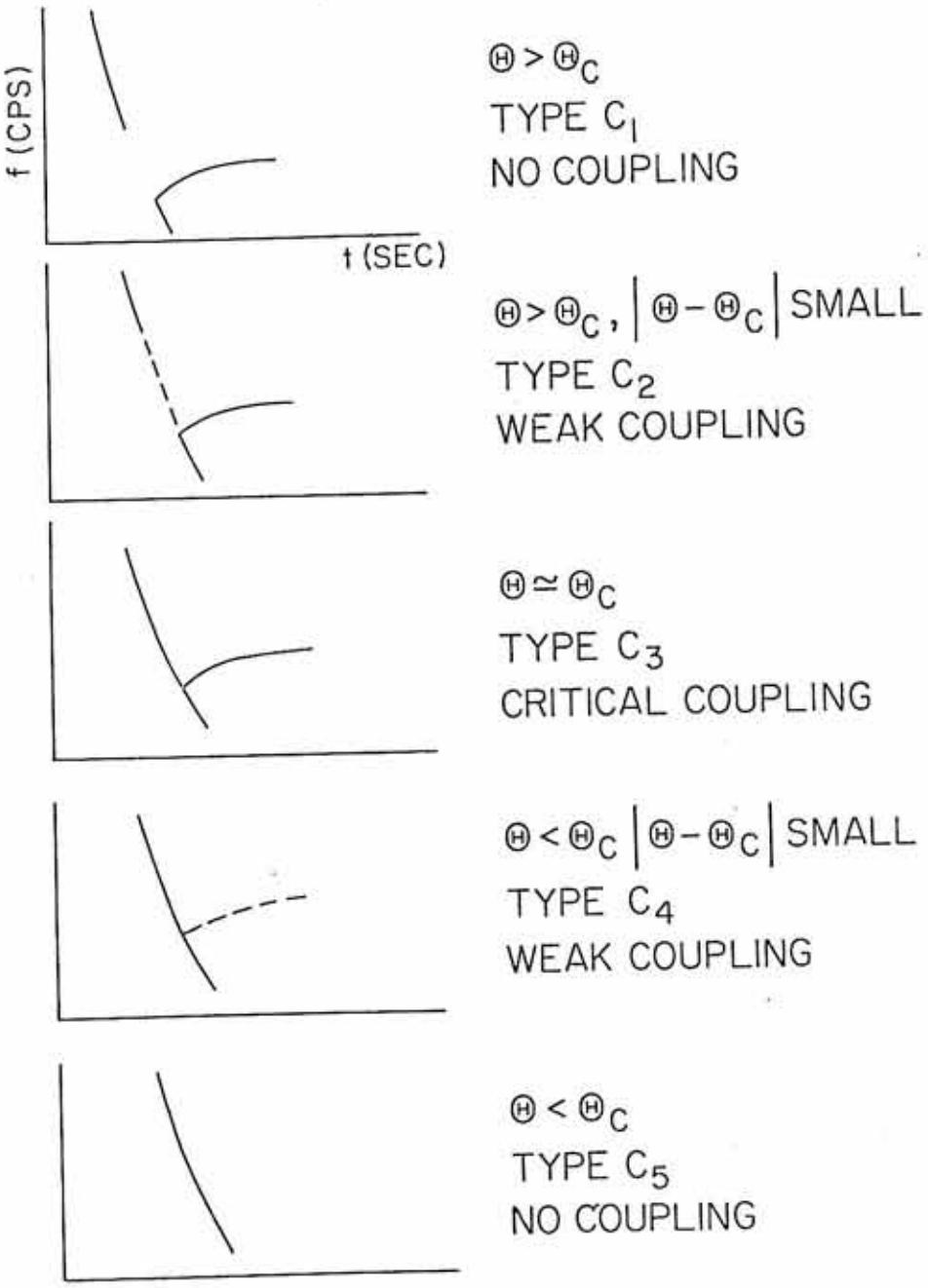

FIGURE 6

Figure 7 Injun 3 spectrogram samples of the coupling classification.

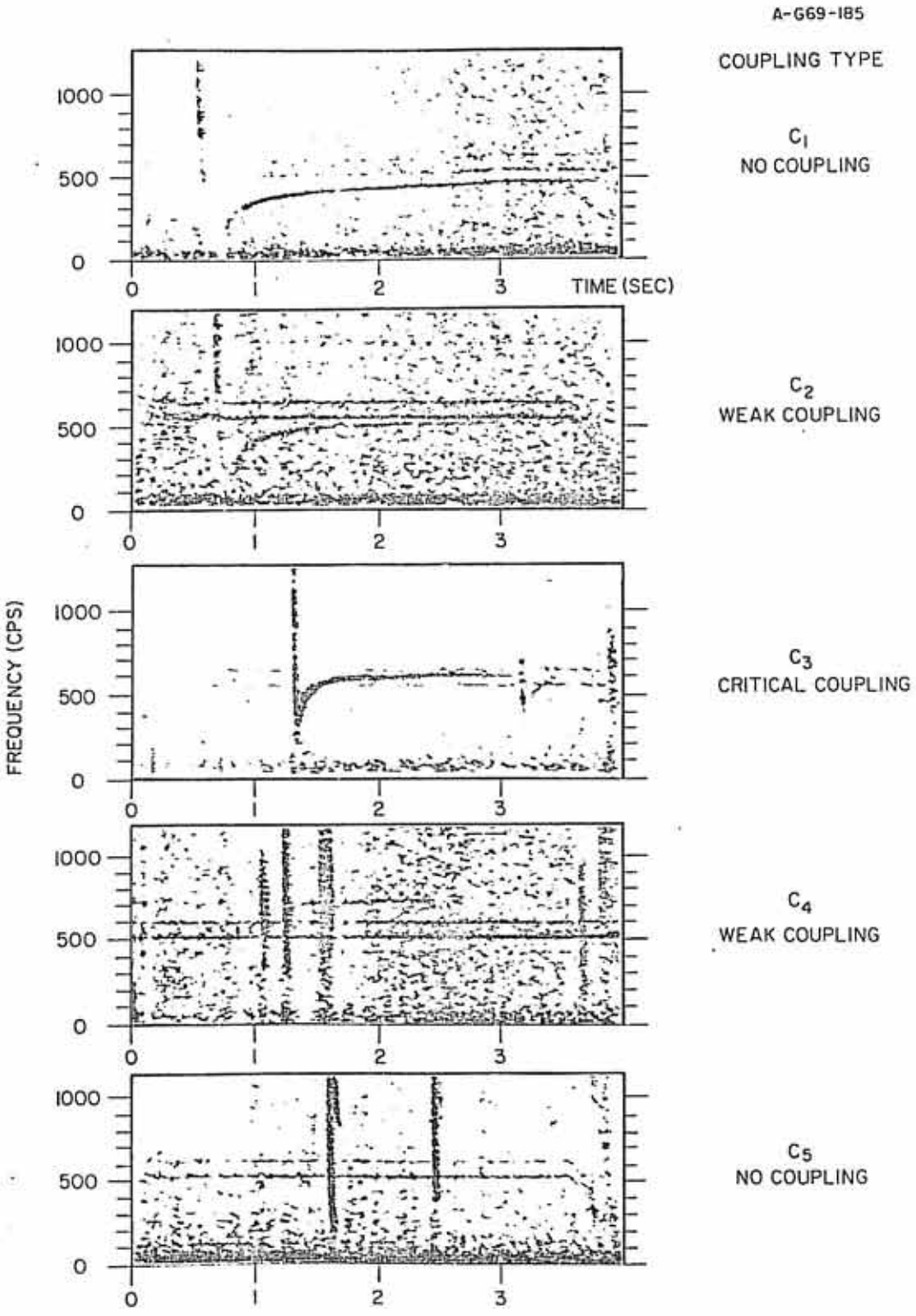
A-G69-185
COUPLING TYPE
C1
NO COUPLING
C2
WEAK COUPLING
C3
CRITICAL COUPLING
C4
WEAK COUPLING
C5
NO COUPLING
FREQUENCY (CPS)
TIME (SEC)
1000
500
0
0
1
2
3

FIGURE 7

Figure 8 a Number of spectrogram samples taken in terms of local time and magnetic latitude. The definitions of winter-night and summer-day for Injun 3 passes is given. AA' is a single Injun 5 pass. Cross-hatched area is the approximate region covered by OGO-2 October 14-24, 1965.

A-G69-238

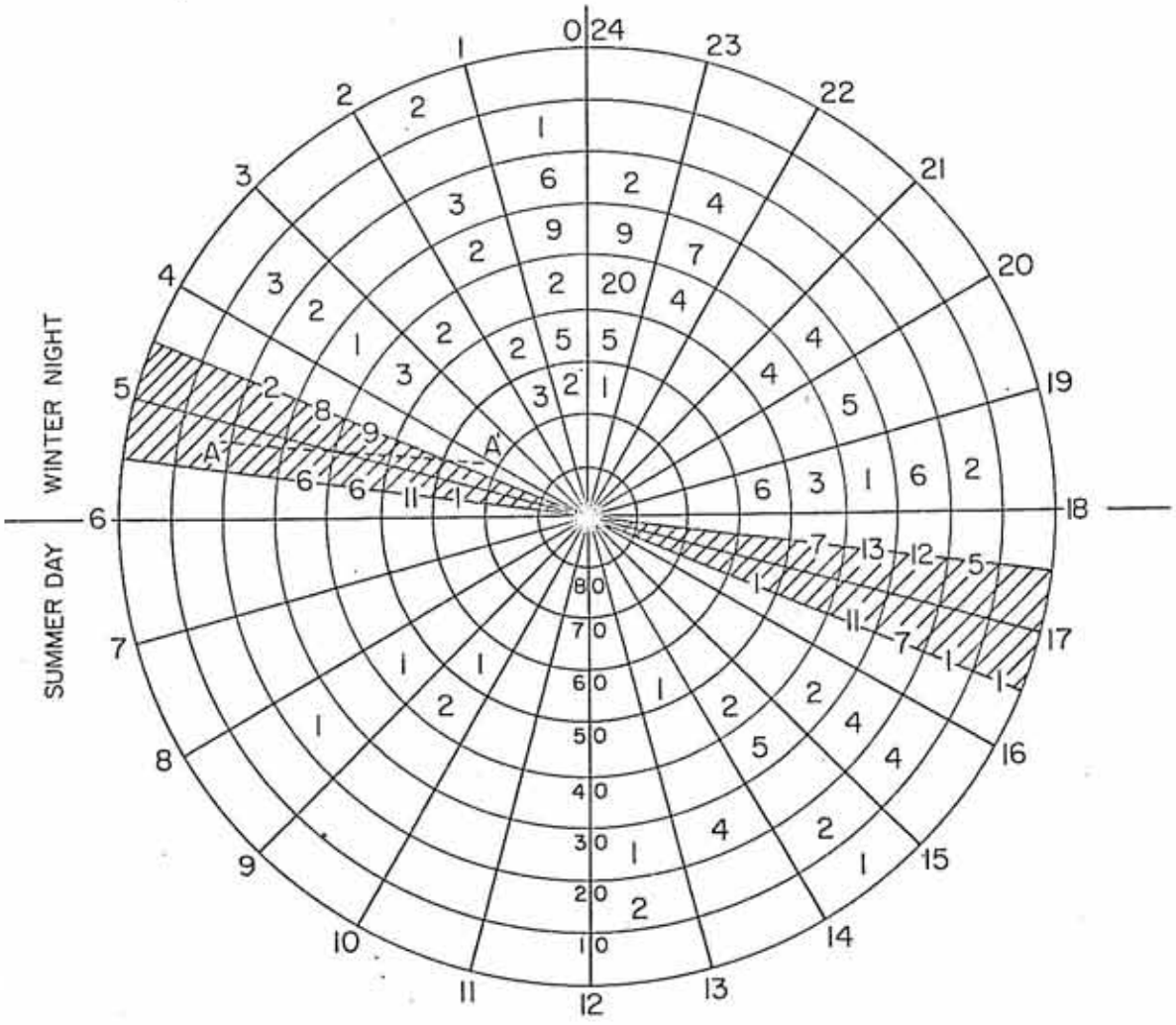

INJUN 3 PASS NOS.	DATES YR-MO-DA	NORTHERN HEMISPHERE	SOUTHERN HEMISPHERE
97 – 1211	62-12-21 → 63-3-21	WINTER	SUMMER
2363 – 3514	63-6-21 → 63-9-21	SUMMER	WINTER

DAY / NIGHT } IS DEFINED AS { 0700-1800 HRS LT / 1900-0600 HRS LT

FIGURE 8A

Figure 8b Number of coupling type samples in terms of altitude and magnetic latitude.

A-G69-237

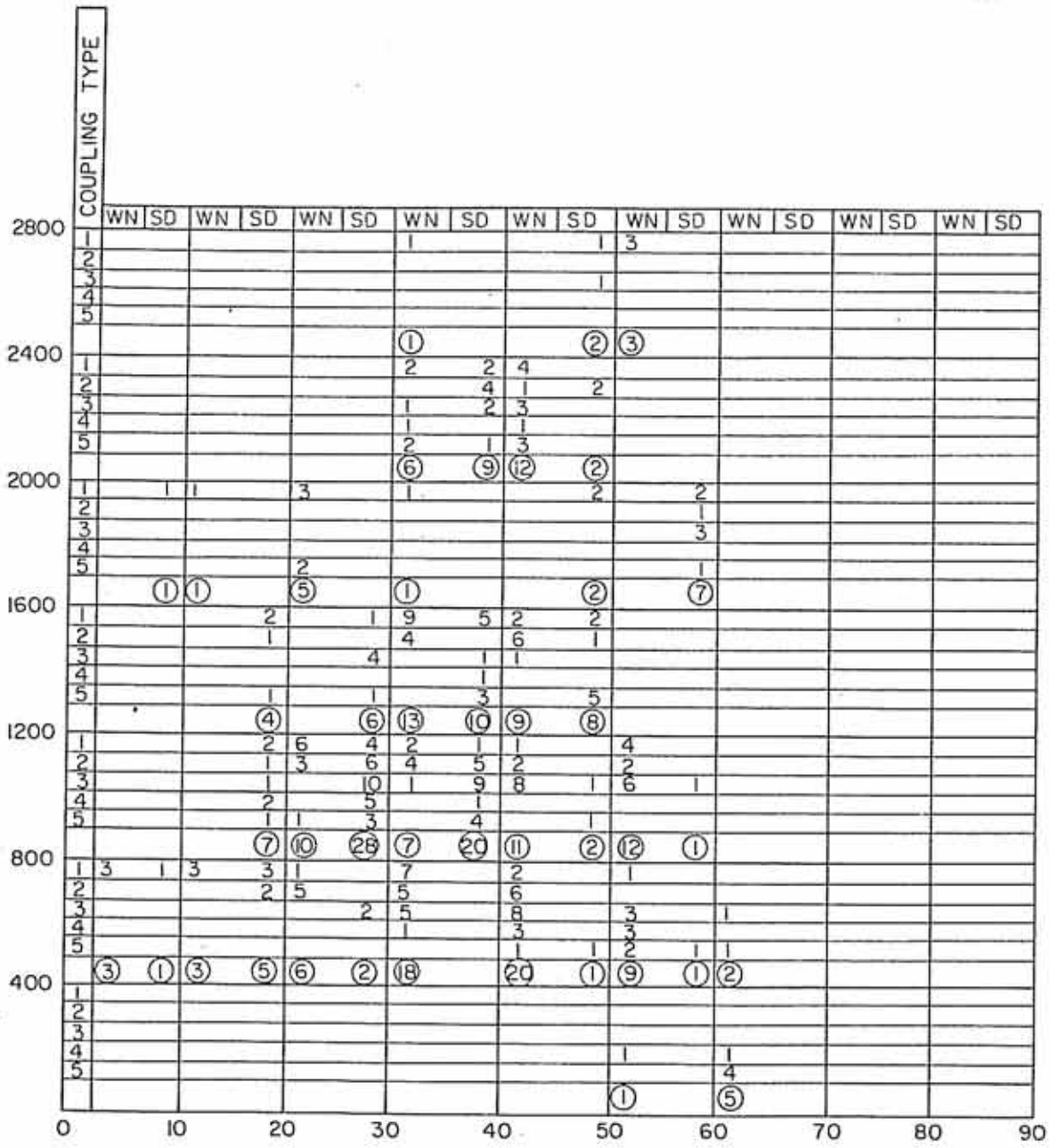

FIGURE 8B

Figure 9 Winter-night variation of coupling type with altitude and magnetic latitude. Dotted lines indicate no data were available in that region. The dashed line marked C_5 indicates samples not used to construct full lines. AA' is a single pass of Injun 5 in which the coupling types indicated by the subscript of C_i were observed. This shows the transitions occurring over a typical mid-latitude pass.

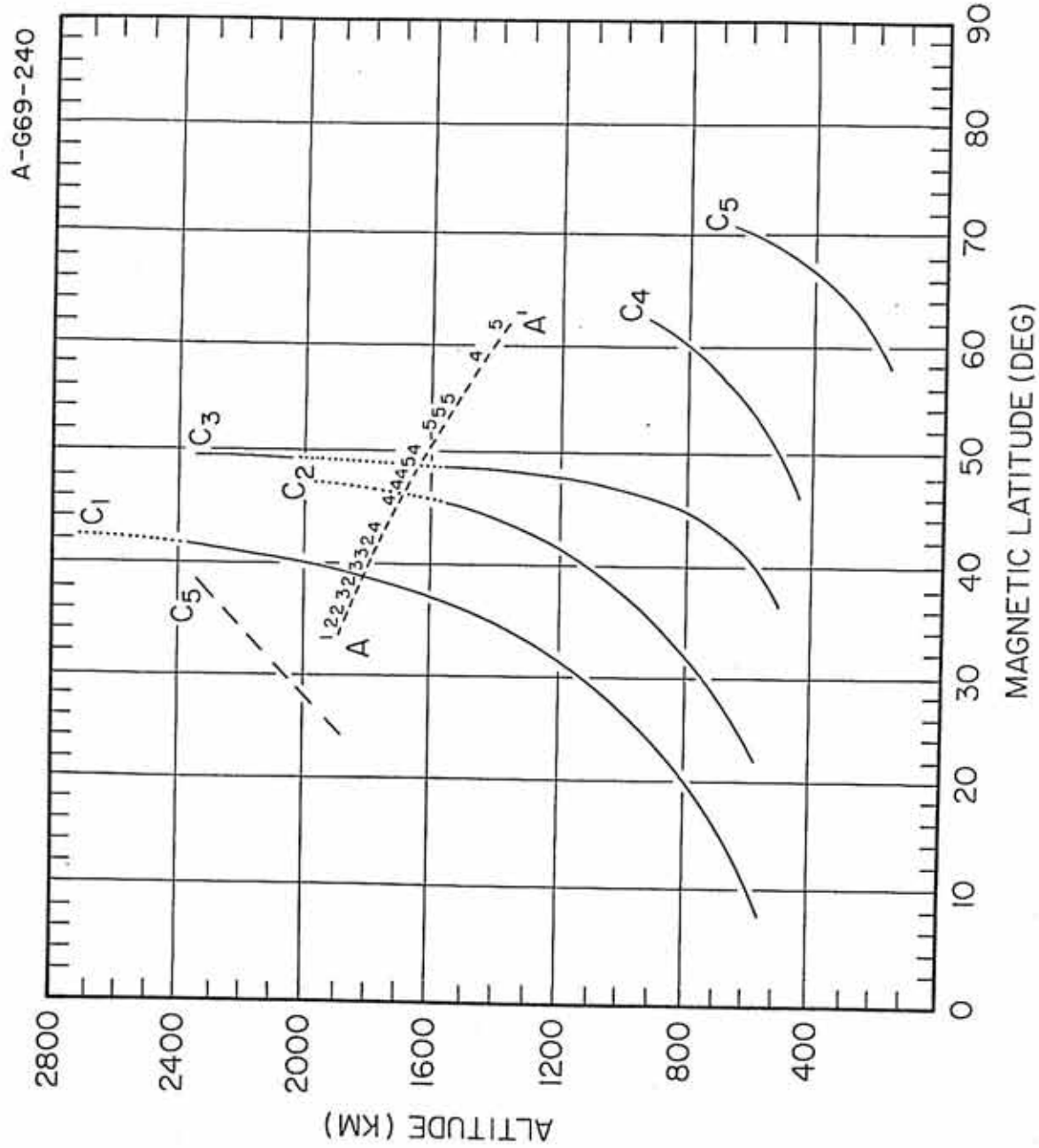
A-G69-240
ALTITUDE (KM)
2800
2400
2000
1600
1200
800
400
MAGNETIC LATITUDE (DEG)
0
10
20
30
40
50
60
70
80
90
C1
C2
C3
C4
C5
C5
A
A'
1
2
2
3
2
3
3
2
4
4
4
4
5
4
5
5
5
4
5

FIGURE 9

Figure 10 Summer-day variation of coupling type with altitude and magnetic latitude. Dotted lines indicate no data were available in that region. Dashed line marked C_3 indicates samples not used to construct full lines.

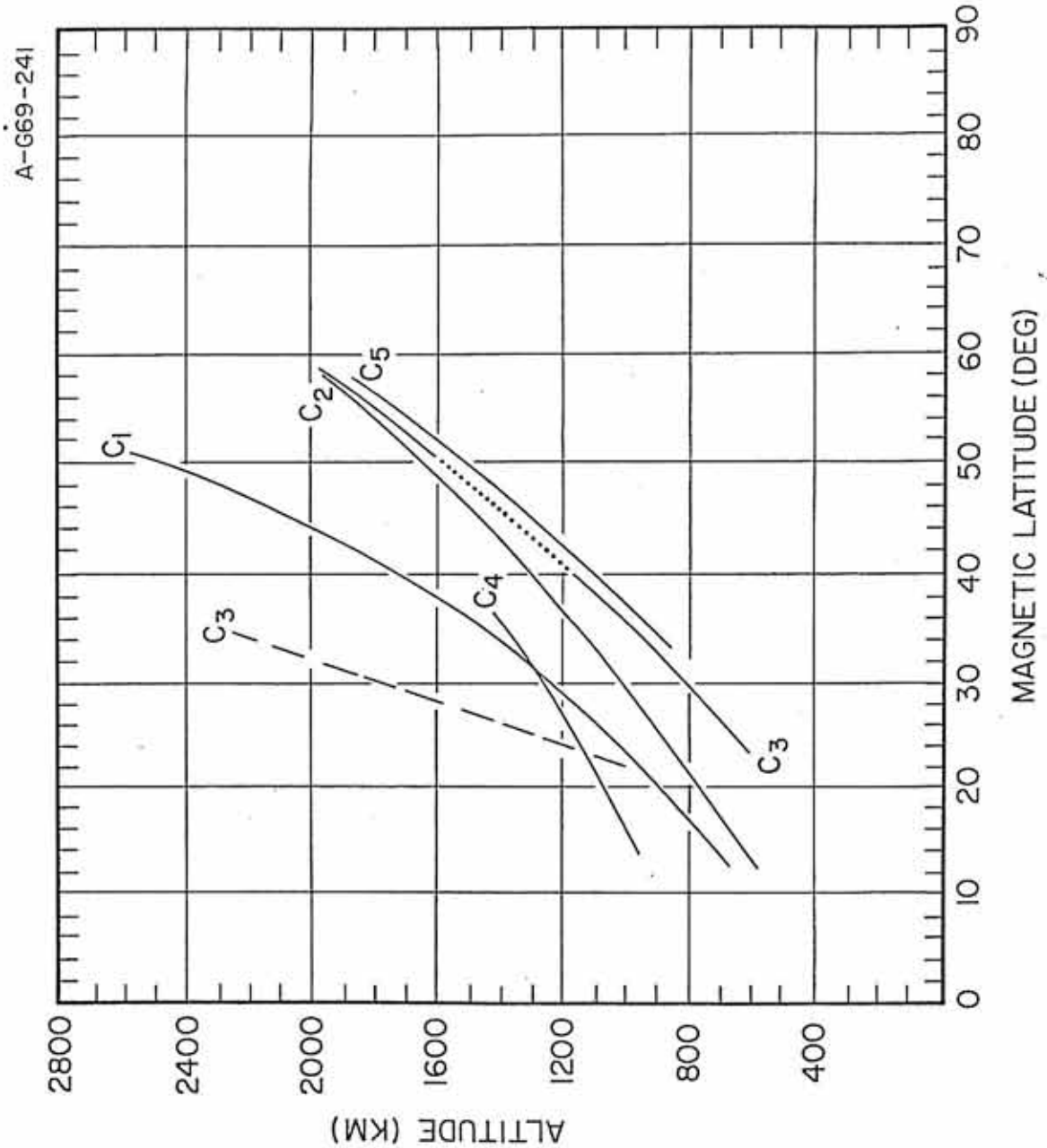
A-G69-241
ALTITUDE (KM)
2800
2400
2000
1600
1200
800
400
MAGNETIC LATITUDE (DEG)
0
10
20
30
40
50
60
70
80
90
C1
C2
C3
C4
C5
C3

FIGURE 10

Figure 11 Observed parameter surfaces L = ∞, D = 0 for winter-night and 10° magnetic latitude intervals.

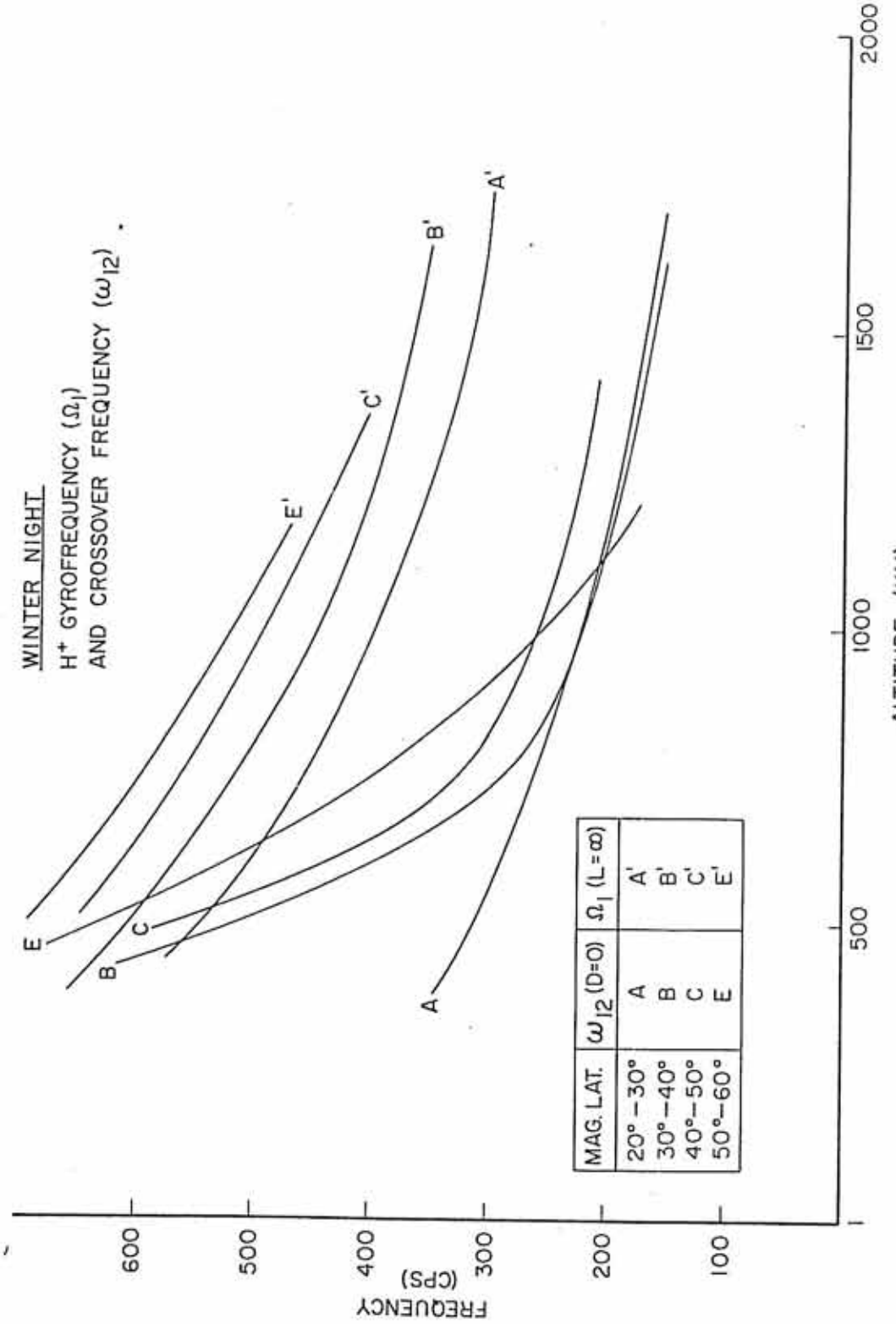
A-669-175
WINTER NIGHT
H+ GYROFREQUENCY (Ω1)
AND CROSSOVER FREQUENCY (ω12)
FREQUENCY (CPS)
ALTITUDE (KM)
100
200
300
400
500
600
500
1000
1500
2000
A
B
C
E
A'
B'
C'
E'
MAG. LAT. | ω12 (D=0) | Ω1 (L=∞)
20°–30° | A | A'
30°–40° | B | B'
40°–50° | C | C'
50°–60° | E | E'

FIGURE 11

Figure 12 Observed parameter surfaces $L = \infty$, $D = 0$ for summer-day and 10° magnetic latitude intervals.

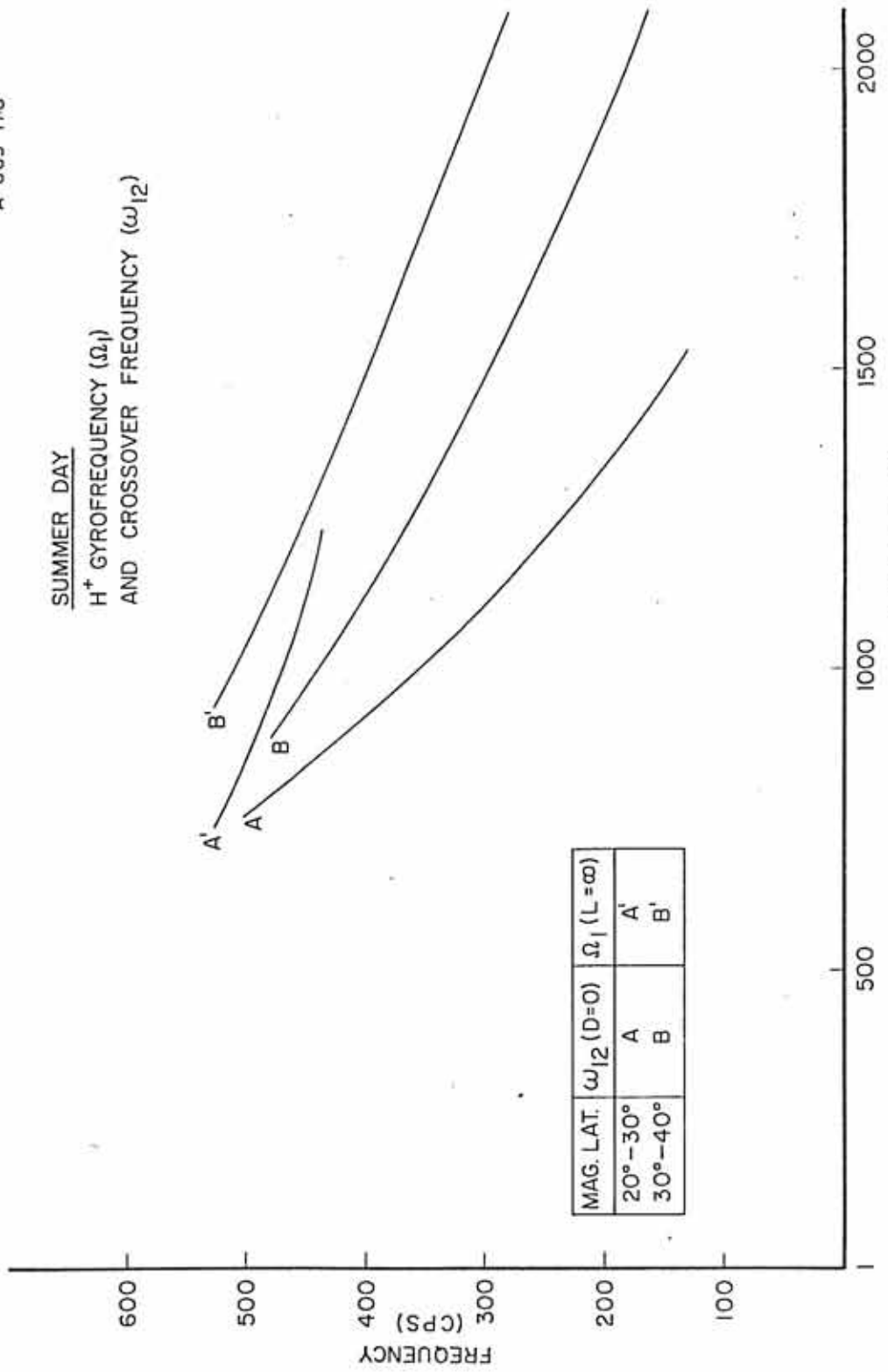
A-669-176
SUMMER DAY
H+ GYROFREQUENCY (Ω1)
AND CROSSOVER FREQUENCY (ω12)
FREQUENCY (CPS)
600
500
400
300
200
100
1
500
1000
1500
2000
ALTITUDE (KM)
A'
A
B
B'
MAG. LAT. | ω12 (D=0) | Ω1 (L=∞)
20°–30° | A | A'
30°–40° | B | B'

FIGURE 12

Figure 13 Observed parameter surfaces $L = \infty$, $D = 0$ for winter-night in the range 30° - 40° magnetic latitude. This shows typically the scatter of points measured for Ω_1, ω_{12}, Ω_c.

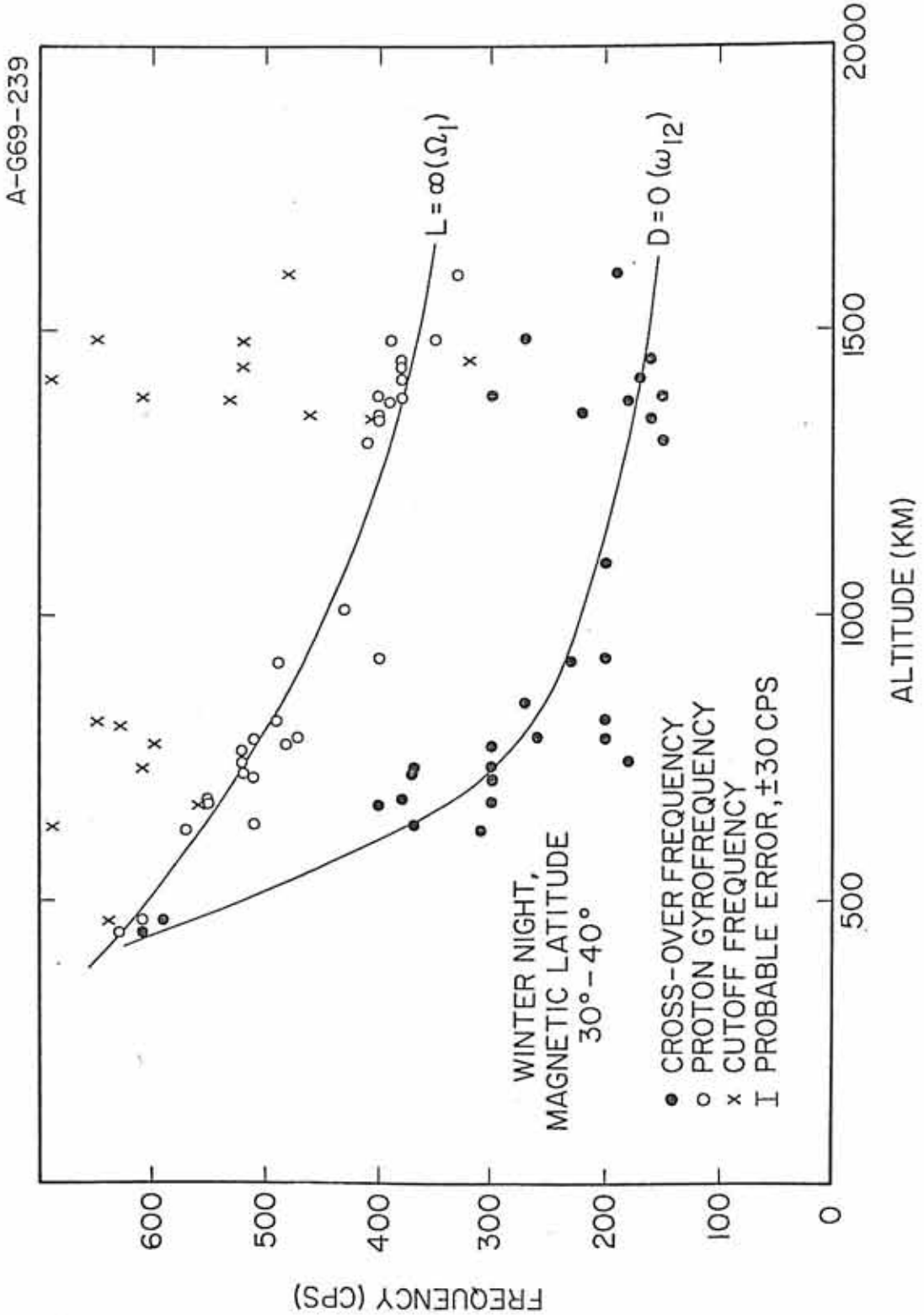
A-G69-239
L = ∞ (Ω1)
D = 0 (ω12)
WINTER NIGHT,
MAGNETIC LATITUDE
30°-40°
● CROSS-OVER FREQUENCY
○ PROTON GYROFREQUENCY
× CUTOFF FREQUENCY
I PROBABLE ERROR, ±30 CPS
FREQUENCY (CPS)
0
100
200
300
400
500
600
ALTITUDE (KM)
500
1000
1500
2000

FIGURE 13

Figure 14 Schematic diagram showing transitions at the parameter surfaces $L = \infty$, $D = 0$, $L = 0$ for upgoing and downgoing whistlers and for three wave normal angles.

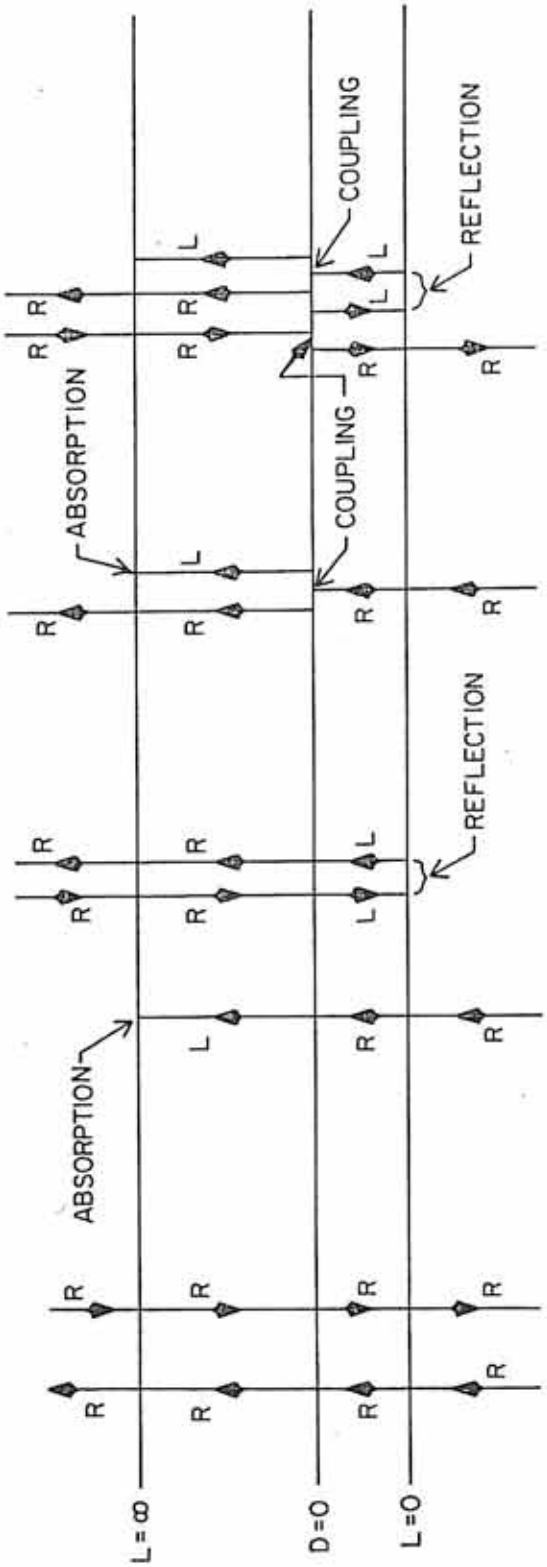
A-G69-323
COUPLING
REFLECTION
ABSORPTION
COUPLING
REFLECTION
ABSORPTION
L
R
L=∞
D=0
L=0
θ = θc
θ > θc
θ < θc

FIGURE 14

Figure 15 Top photograph: Proton whistler partially formed near the cross-over frequency. Center and bottom photographs: Helium whistlers visible below proton whistlers.

A-G69-186

INCOMPLETE PROTON
WHISTLER

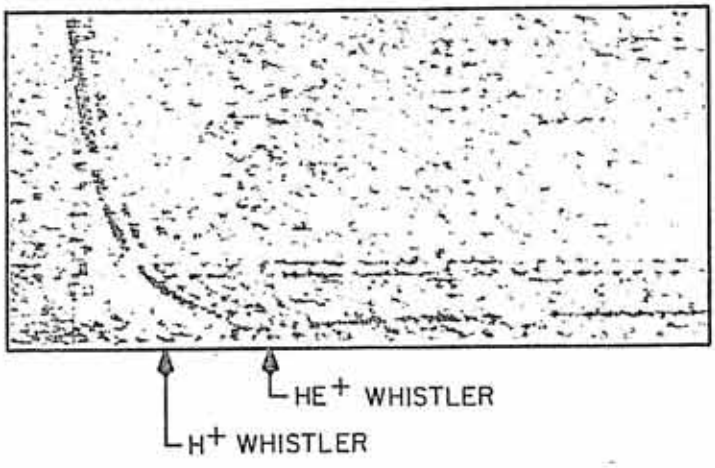

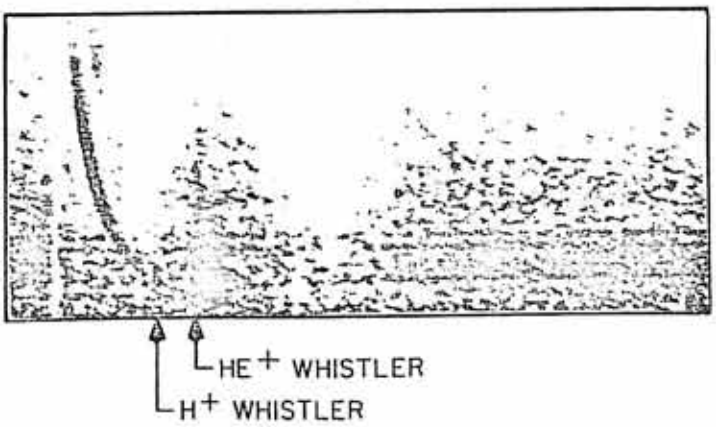

FIGURE 15